Cellulose (2016) 23:3341–3354
DOI 10.1007/s10570-016-1013-z

ORIGINAL PAPER

Unique nanobrick wall nanocoating for flame-retardant cotton fabric via layer-by-layer assembly technique

Fei Fang · Bin Tong · Tianxiang Du · Xian Zhang · Yuedong Meng · Xianglan Liu · Xingyou Tian

Received: 28 March 2016 / Accepted: 11 July 2016 / Published online: 19 July 2016

Abstract Unique quadlayer assembly film of polyhexamethylene guanidine phosphate (PHMGP)/ammonium polyphosphate (APP)/PHMGP/α-zirconium phosphate (α-ZrP) was constructed on cotton fabric to achieve excellent flame-retardant modification. X-ray diffraction and attenuated total reflection Fourier transform infrared spectroscopy confirmed that PHMGP, APP, and α-ZrP grew linearly in the layer-by-layer assembly process. Thermogravimetric analysis was carried out to assess the thermal stability of the coated fabric, and the relevant results showed that cotton fabric were effectively protected by the assembly coating during burning. The microscale combustion calorimetry results indicated that the coated fabric showed smaller values of the peak heat release rate and total heat release than the uncoated one. Characterizations of burning behaviors of all fabrics in vertical configuration revealed that the nanobrick wall coating obviously decreased the burning time, thoroughly eliminated the afterglow phenomenon, and significantly enhanced the residue char left after burning. Moreover, the unique nanobrick wall coating provides an enhanced flame-retardant effect as compared to the PHMGP/APP, PHMGP/α-ZrP and APP coatings. The scanning electron micrograph and Fourier transform infrared spectra of the residue chars revealed that the excellent flame retardancy of the coated cotton was attributed to the catalytic charring of the intumescent component and the protection of the unique nanobrick wall as an reinforced barrier layer during burning.

Keywords Layer-by-layer assembly · Nanobrick wall · Coating · Flame retardant · Cotton fabric

Fei Fang and Bin Tong have contributed equally to this work and should be considered co-first authors.

F. Fang · Y. Meng
Institute of Plasma Physics, Chinese Academy of Sciences, Hefei 230031, People's Republic of China

F. Fang · B. Tong · X. Zhang (✉) · X. Liu · X. Tian (✉)
Institute of Applied Technology, Hefei Institutes of Physical Science, Chinese Academy of Sciences, Hefei 230088, People's Republic of China
e-mail: xzhang@issp.ac.cn

X. Tian
e-mail: xytian@issp.ac.cn

T. Du
School of Material Science and Engineering, Shandong University, Jinan 250002, People's Republic of China

Introduction

Owing to the excellent characteristics of the smooth handle, good breathability and hygroscopicity, cotton fabric has been widely applied in clothing, furniture and industrial textiles, and so on (Wakelyn et al. 2007). However, its intrinsic nature of flammability

can easily result in fire, which can pose immediate danger to human health and environmental quality. To date, various flame-retardant treatments, such as nanoparticle adsorption (Alongi et al. 2011b, 2012a; Horrocks et al. 2011; Liu et al. 2008), surface chemical grafting (Reddy et al. 2005; Yuan et al. 2012) and sol-gel technology (Alongi et al. 2011a, 2012b), have been applied in textile fabrics to improve the flame-retardant properties. However, these strategies have the disadvantage of limited flame-retardant performance or complex chemical processes under harsh conditions, which could restrict further industrial applications.

Recently, polymer-clay layer-by-layer (LBL) assembly coating, as a frontier of nanotechnology, has been applied to conferring flame-retardant performance to various textile fabrics. This technique, as an evolution of the nanoparticle adsorption process (Cobo et al. 2006), involves simple alternate immersion of the substrate into an oppositely charged (usually water-based) polyelectrolyte solution or nanoparticle dispersion (Berndt et al. 1992; Decher and Hong 1991; Tang et al. 2003). As a result, the polymer-clay assembled films have a nacre-like nanobrick wall microstructure, which could lead to the superior fire-resistant property (Liu et al. 2011; Sehaqui et al. 2013; Walther et al. 2010; Yao et al. 2010). In addition to the flame retardance, by incorporating different building materials, these multilayers have been demonstrated to have various performances, including electrical conductivity (Chen et al. 2008; Park et al. 2010), anti-ultraviolet (Dawidczyk et al. 2008; Guin et al. 2015), mechanical (Finnemore et al. 2012; Wang et al. 2012) and barrier properties (Stevens et al. 2014; Yang et al. 2013). The first attempt on cotton fabric was carried out in 2009 by alternately depositing cationic branched poly(ethylenimine) and negatively charged laponite nanoplatelets (Li et al. 2009). This polymer/clay assembly could significantly improve the thermal stability of cotton fabric. Pursueing this research, various nanoplatelets have been introduced in these nanobrick wall coatings, such as sodium montmorillonite (Cain et al. 2014b; Huang et al. 2012a; Kim et al. 2012; Li et al. 2010, 2013; Xu et al. 2014), layered double hydroxide (Li et al. 2015) and alpha-zirconium phosphate (α-$Zr(HPO_4)_2{\cdot}H_2O$, α-ZrP) (Carosio et al. 2011), and so on. Although the flame-retardant results appeared promising to some extent, these nanobrick wall coatings were unable to fully suppress the flame only through the deposition of nanoparticles.

Shortly after these inorganic LBL nanocoatings, another flame-retardant system, an organic intumescent coating was designed by combining cationic poly(allylamine) with anionic poly(sodium phosphate) (PSP), showing a powerful flame-resistant effect on cotton fabric (Li et al. 2011). It is well known that intumescent coatings have an excellent flame-retardant effect on textiles by the powerful alliance of an acid source, carbon source and blowing agent (Kandola et al. 2001), showing different flame-retarding ingredients and mechanisms with an inorganic LBL coating. When exposed to fire, intumescent coating promotes the formation of thermally stable intumescent char, which acts as a barrier layer separating the underlying matrix from outside heat and oxygen (Apaydin et al. 2014; Cain et al. 2014a; Carosio et al. 2013; Huang et al. 2012b; Laufer et al. 2012; Zhang et al. 2013). Recently, our research group first employed polyhexamethylene guanidine phosphate (PHMGP) coupled with ammonium polyphosphate (APP) in an intumescent coating, which had a perfect flame-retardant effect on cotton fabric (Fang et al. 2015a).

Lately, the inorganic nanomaterial montmorillonite (MMT) and organic intumescent components (poly(allylamine hydrochloride) (PAH) and PSP) were combined in a single coating system, which was demonstrated by Grunlan (Cain et al. 2013). This unique nanobrick wall collected the advantages of two flame-retardant systems (an inorganic insulating layer and organic intumescent coating), which could be considered as an important advance in LBL flame-retardant coatings. As expected, this PAH/PSP/MMT trilayer has been proved to be an effective thermal insulating layer, which could completely shut down melt dipping and reduce the heat release of polyurethane foam. Moreover, another nanobrick wall coating, based on the diffusion of PSPs in PAH-MMT multilayer films, has also been proved to possess excellent fire-resistant, mechanical and gas barrier properties (Laachachi et al. 2011). However, there was no report about the unique nanobrick wall coating used for flame-retardant cotton fabric.

In the present work, we combine the intumescent ingredients PHMGP and APP with α-ZrP nanoplatelets in an effort to obtain an excellent flame-retardant effect on cotton fabric. In this scenario, PHMGP and

APP are used as the polymer mortars to bind α-ZrP nanoplatelets forming a reinforced nanobrick wall structure as a thermal insulating physical barrier layer during burning. As a well-known MMT-like layered nanoplatelet, α-ZrP possesses a high ion-exchange capacity, narrow particle size distribution and controllable aspect ratio (Trobajo et al. 2000; Wang et al. 2003). Thus, it has been identified as a promising alternative nanoplatelet to MMT to develop polymer/layered inorganic nanocomposites (Hongdian and Wilkie 2011). What is more, as a "solid acid," α-ZrP can catalyze dehydrogenation of the polymer and further acts as good synergistic agents with an intumescent fire retardant (Liu et al. 2013; Ullah and Ahmad 2014; Weiyi et al. 2014). Additionally, α-ZrP nanoplatelets can function as mechanical and flame-retardant reinforcements on several polymer matrixes at relatively low loading (10 %) (Sue et al. 2004; Wu et al. 2010). Specifically, as a kind of negatively charged nanoplatelet, α-ZrP can be assembled with the cationic polymer PHMGP, which can be further assembled with anionic APP. In this way, PHMGP/APP/PHMGP/α-ZrP quadlayer nanoarchitecture is constructed on cotton fabric step by step. The assembly coating growth was monitored by X-ray diffraction (XRD) and attenuated total reflection Fourier transform infrared (ATR-FITR) spectroscopy. The flame-retardant effect of the assembly coating on cotton fabric was evaluated by thermogravimetric analysis (TGA), microscale combustion calorimetry (MCC) and the vertical flammability test (VFT).

Experimental section

Materials

Cotton fabric with a density of 230 g m^{-2} was purchased from an online fabric store. Polyhexamethylene guanidine phosphate (PHMGP, $(C_7H_{15}N_3 \cdot H_3PO_4)n$, polymerization degree >60, 25 wt% in water) was obtained from Shanghai Scunder Industry Co., Ltd. Ammonium polyphosphate (APP, $(NH_4PO_3)n$, polymerization degree >1000) was received from Shandong Shian Chemical Co., Ltd. α-ZrP ($Zr_3(PO_4)_4$) was synthesized by adding 3 ml (1.6 g ml^{-1}) zirconium oxychloride octahydrate drop by drop to 45 ml (3.0 M) phosphoric acid at 200 °C for 72 h. The detailed synthetic process of α-ZrP can be found elsewhere (Shuai et al. 2013). Figure 1 shows the morphology of α-ZrP nanoplatelets with width and thickness of about 500 and 50 nm. All self-assembled products were prepared in 0.1 wt% aqueous solutions or suspension for LBL assembly; the pH values for PHMGP and APP solutions and α-ZrP suspension were adjusted to 7.0, 10.0 and 7.0, respectively.

Layer-by-layer process

Cotton fabric was successively immersed into cationic PHMGP and anionic APP solutions and then successively immersed into cationic PHMGP solution and anionic α-ZrP suspension. After each immersion step, the fabric was rinsed with deionized water and dried in air at 60 °C for 30 min. A first quadlayer (QL) was obtained after these four immersion steps. The immersion period for the primer QL was 5 min to promote the deposition, and the subsequent immersion only lasted for 1 min. The final coated fabrics were acquired until the desired QL number (5, 10 and 20) was achieved. The add-ons for the 5-, 10- and 20-QL-coated fabrics were 1.2, 3.7 and 5.4 wt%, respectively, as shown in Table 1. Additionally, the PHMGP/APP-, PHMGP/α-ZrP- and pure APP-coated fabrics with 1.3 wt% add-on were prepared according to the above similar method.

Characterization

ATR-FTIR spectra of the uncoated and coated fabrics and FTIR spectra of the char residues of the coated fabrics after burning were collected using a Nicolet 8700 spectrometer (Thermo Nicolet Corp., USA). The spectrometer was equipped with a Ge crystal for the recording of ATR-FTIR spectra. TGA was conducted on a Pyris 1 Thermogravimetric Analyzer (PerkinElmer, USA) in the temperature range of 50–600 °C, at the heating rate of 10 °C min^{-1}, in air atmospheres. MCC was executed on an FAA microscale combustion calorimeter (FTT Ltd., USA) in the temperature range of 50–600 °C, at the heating rate of 1 °C s^{-1}, with the oxygen/nitrogen flow rate of 20/80 ml/ml. VFT was performed on an AG5100A Horizontal Vertical flame tester (Zhuhai Angui Testing Instrument Co., Ltd.). The fabrics (120 × 37 mm^2) were exposed to the flame (height: 40 mm ± 2 mm, gas: methane) for 12 s. The surface morphologies of the neat and coated fabrics and the char residues of the coated fabrics were analyzed by a

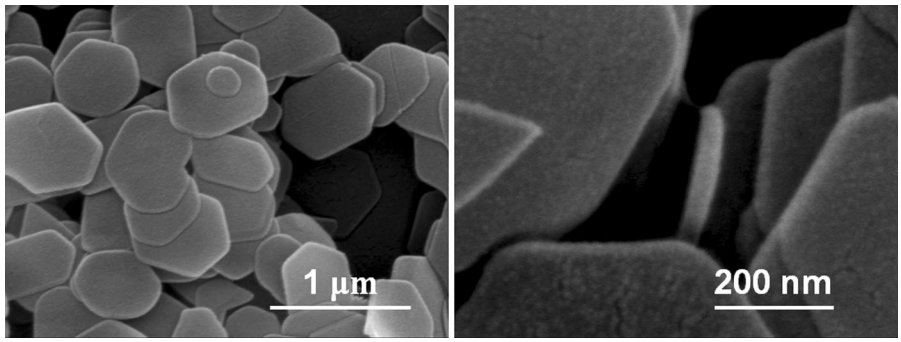

Fig. 1 The SEM micrographs of α-ZrP nanoplatelets

Table 1 The TG data of the uncoated and coated fabrics in air

Sample	Add-on (wt%)	T_{onset} (°C)	T_{max1} (°C)	Residue at T_{max1} (wt%)	T_{max2} (°C)	Residue at 600 °C (wt%)
Uncoated	–	305	368	54.4	501	1.5
5 QL	1.2	288	334	66.2	526	4.4
10 QL	3.7	288	332	66.3	527	5.4
20 QL	5.4	287	331	70.4	530	9.7

Sirion 200 field emission scanning electron microscope (SEM) (FEI Corp., USA). The Zr and P element mapping of the nanobrick wall-coated fabrics was performed by an energy-dispersive X-ray (EDX) detector.

Results and discussion

Surface composition

The surface compositions of the uncoated and coated fabrics were explored by XRD and ATR-FTIR spectroscopy, and the corresponding spectra are shown in Fig. 2a, b, respectively. The XRD pattern of pure cotton exhibits five characteristic peaks of crystalline cellulose at $2\theta = 15.0°$ (101), 16.7° (101), 20.4° (021), 22.8° (002) and 34.7° (040) (see Fig. 2a) (Ford et al. 2010). After the introduction of the assembly coating, three new signals emerge in the XRD patterns at $2\theta = 11.9°$ (002), 20.4° (110) and 25.7° (112) attributed to the characteristic peaks of α-ZrP (Shuai et al. 2013), suggesting that α-ZrP nanoplatelets are successfully deposited on cotton fabric. Additionally, the characteristic peak intensities of α-ZrP and cellulose become stronger and weaker with increasing QLs, respectively, indicating that the α-ZrP amount grows gradually in the LBL assembly process.

Figure 2b shows the ATR-FTIR spectra obtained for the uncoated and coated fabrics. The spectrum of the pure cotton exhibits the characteristic signals of cellulose. It contains the O–H absorption around 3337 cm^{-1}, C–H absorption peaks at 1312 and 1369 cm^{-1} and a C–O–C absorption band from 950 to 1200 cm^{-1} (Chung et al. 2004). With the increase of QL number, these characteristic signals are attenuated as a result of the shielding action of the assembly coating. Beyond that, some new signals appear in the spectra of the coated fabrics. As shown in Fig. 2, a strong peak is observed at 1636 cm^{-1} because of the N–H bend vibration in PHMGP (Zhang et al. 1999). Another two unique signals appear at 1245 and 858 cm^{-1} from the P=O and P–O–P vibration in APP (Zheng et al. 2014). Additionally, three emerging sharp peaks at 1039, 1001 and 962 cm^{-1} are assigned to the P–O stretching bands (Hajipour and Karimi 2014; Tian et al. 2010), further indicating the presence of α-ZrP nanoparticles in the assembly coating. These results suggest that the self-assembly materials (PHMGP, APP and α-ZrP) used in the LBL process are all deposited on cotton fabric.

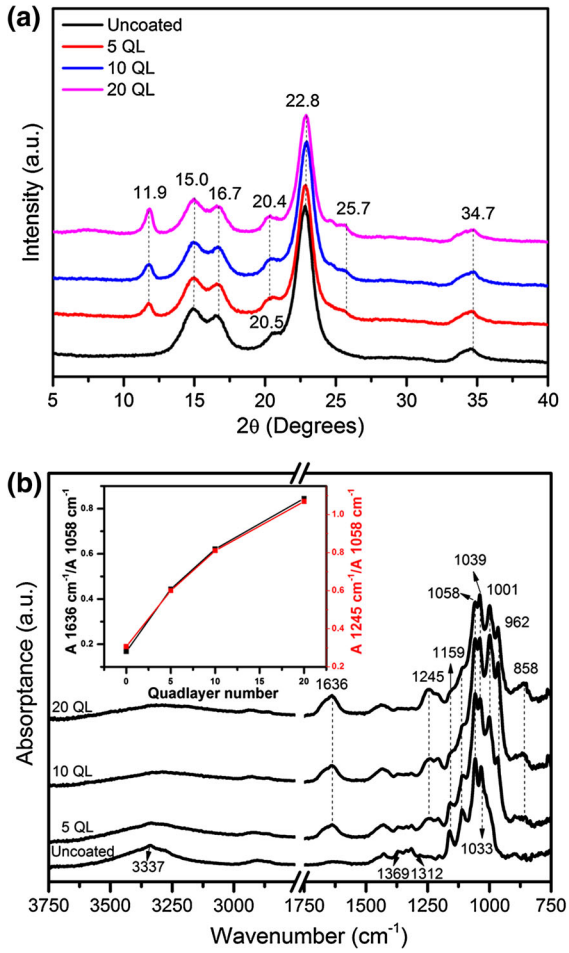

Fig. 2 The XRD patterns (**a**) and ATR-FTIR spectra (**b**) of the uncoated and coated fabrics. The *inset* shows the relative intensities (A1636 cm^{-1}/A1058 cm^{-1}, A1245 cm^{-1}/A1058 cm^{-1}) as a function of the QL number

To further monitor the LBL growth of the nanobrick wall architecture, the absorption intensity at 1058 cm^{-1} of C–O–C in cellulose was chosen as the reference. Because the P–O signals of α-ZrP at 1039, 1001 and 962 cm^{-1} are overlapped with the absorption band of cellulose, the collected absorption values are not absolutely attributed to the absorption of P–O. In view of this, we calculate the relative intensities (N–H/C–O–C intensity ratio: A1636 cm^{-1}/A1058 cm^{-1}, P=O/C–O–C intensity ratio: A1245 cm^{-1}/A1058 cm^{-1}) as a function of the QL number (see inset). It can be seen that the relative intensities increase approximately linearly with the growth of the QL number from 5 to 20, indicating that the nanobrick wall coating grows approximately linearly in the LBL process.

To study the surface morphologies of the cotton fabrics, all fabrics were photographed by SEM. As shown in Fig. 3, the uncoated fiber has a very clean and smooth surface as compared to the coated samples. It is surprising that with only a 5-QL coating the α-ZrP nanoplatelets mount layer upon layer forming a nanobrick wall architecture on the fiber surface. The only downside is that there are still some smooth spots without any α-ZrP nanoplatelets, which could be because of insufficient immersion during the LBL process. As the QL number increases to 10, the LBL structure becomes more uniform with respect to the 5 QLs. It is noteworthy that the assembly coatings do not fill the spaces between cotton fibers for the 5- and 10-BL-coated fabrics, so the handle feelings of these fabrics cannot be stiffened drastically by introducing the nanobrick wall coating. In the case of the 20-QL-coated fabric, a relatively perfect brick wall architecture appears on the fiber surface; meanwhile, some fibers begin to bond together, which inevitably results in the stiffening of the fabric. The EDX mapping shows that the Zr and P elements are uniformly distributed on the fiber surface, indicating that the nanobrick wall architecture is coated evenly on the cotton fabric. Additionally, it can be found that the amount of self-assembled materials increases with the growth of QL number.

Thermostability

The thermal decomposition behaviors of the uncoated and coated fabrics were monitored by TGA, as shown in Fig. 4, and the corresponding data were collected in Table 1. Cotton begins to degrade at 305 °C (T_{onset}) and undergoes two decomposition stages, 300–400 and 400–600 °C, in the whole testing process. It shows the maximum decomposition rates at 368 and 501 °C (T_{max}), which involves the depolymerization of cellulose and oxidization of aliphatic char (Alongi et al. 2014), respectively. After TGA, 1.5 wt% residue char is left at 600 °C.

However, the coated fabric shows decreased onset temperature (T_{onset}) and T_{max1}, and the T_{onset} and T_{max1} also decrease with the growth of the QL number. It has been suggested that APP in the assembly coating begins to degrade and generates phosphoric acid. Then, the catalytic sites on α-ZrP and released phosphoric acid from APP at the bottom of the nanobrick wall accelerate the initial decomposition of

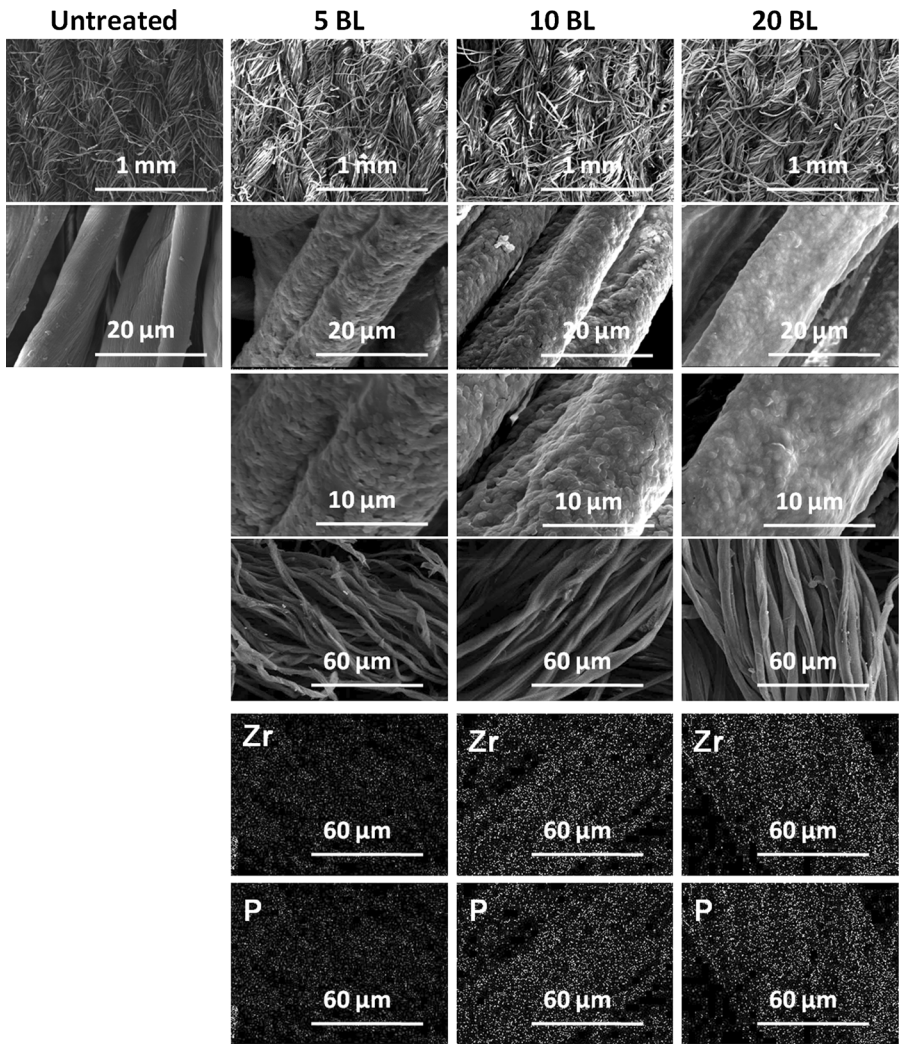

Fig. 3 The SEM images of the uncoated and coated fabrics and and their Zr and P mapping

cotton fabric (Horrocks 2011; Yang et al. 2008). Meanwhile, the catalytic effects can also favor the formation of char, which is thermally stable at high temperature (Carosio et al. 2012). Therefore, the coated fabric shows a significantly decreased mass loss rate with respect to the uncoated fabric. In addition, the residue char of the coated fabric at T_{max1} is much higher than that of the uncoated one, and the char mass increases with the growth of the QL number. The coated fabric also presents a higher T_{max2}, and the value increases further with the growth of the QL number. After TGA, the coated fabric leaves more residue at 600 °C than the uncoated one, and the mass of char increases with the QL number. Furthermore, the residue chars left after TGA are much higher than the coating increment on cotton fabric. These results indicate that the underlaying cotton substrate is effectively protected by the nanobrick wall coating, and the protective effect increases with the growth of the QL number.

In order to further evaluate the flame-retardant effect of the assembly coating, MCC was conducted on the coated fabrics and an uncoated sample. The heat release rate (HRR) curves are shown in Fig. 5, and the collected data are summarized in Table 2. Unlike the thermo-oxidative decomposition behavior, which consists of two stages, cotton's anaerobic pyrolysis exhibits only one peak. By introducing the assembly coating, cotton is pyrolyzed earlier, which can be verified by the decreased onset temperature (T_{onset})

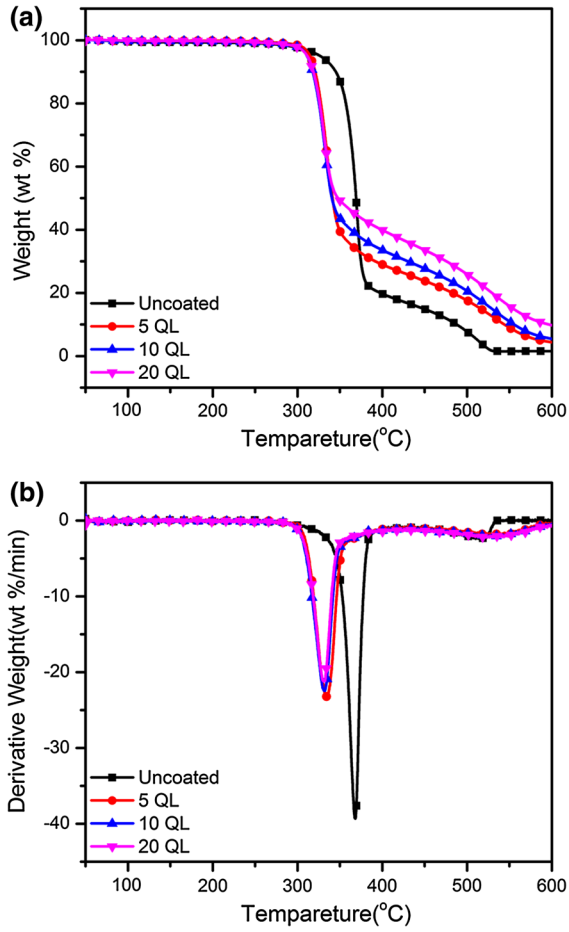

Fig. 4 The TG (**a**) and DTG (**b**) curves of the uncoated and coated fabrics in air

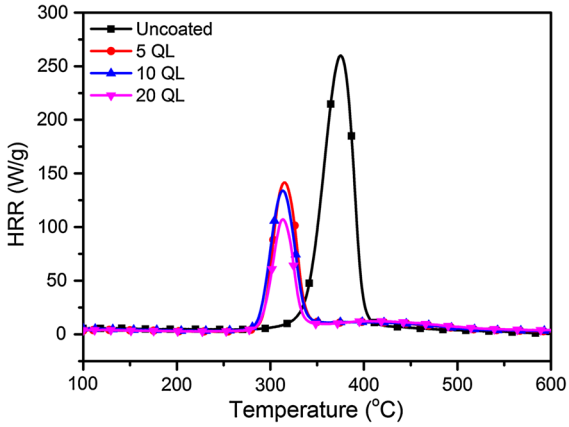

Fig. 5 The MCC curves of the uncoated and coated fabrics

Table 2 The MCC data of the uncoated and coated fabrics

Sample	T_{onset} (°C)	PHRR (W/g)	T_P (°C)	THR (kJ/g)
Uncoated	322	260	375	13.5
5 QL	284	142	316	7.7
10 QL	281	134	313	7.5
20 QL	282	107	313	6.4

and decreased temperature at the peak heat release rate (T_P). This phenomenon agrees with the advanced decomposition behavior in TGA and is attributed to the catalyzed pyrolysis of cellulose by the released phosphoric acid and acid sites on α-ZrP, which can further promote the char formation during testing. What is more, the nanobrick wall as a protective barrier can also suppress the release of combustible volatiles. As a result, the coated fabrics all show a decreased peak heat release rate (PHRR) and total heat release (THR) as key parameters in accessing the flammability of a material, indicating that the nanobrick wall coating can effectively reduce the flammability of cotton fabric. Additionally, the PHRR and THR values decrease with the growth of the QL number, suggesting that the char-forming effect increases with the growth of the QL number. As the QL number increases to 20, the PHRR and THR values decrease to 107 W g^{-1} and 6.4 kJ g^{-1}, reducing by 59 and 53 %, respectively.

Flammability property

The uncoated and coated fabrics were put through vertical flammability tests to evaluate the burning behaviors, and the related data are collected in Table 3. All fabrics were ignited by direct exposure to a methane flame, but a brighter flame appeared on the uncoated fabric, as shown in Fig. 6 at 8 s after ignition. In addition, the uncoated fabric showed 20-s afterglow time and was almost completely consumed after burning. The 5-QL-coated fabric showed a similar burning time as the uncoated one, but the burning time was reduced substantially with increasing QL numbers. The 10 QL burned for 19 s, and as the QL number increased to 20, the burning time was reduced to 14 s, only 2 s longer than the ignition time

Table 3 The collected data of the uncoated and coated fabrics during VFT

Sample	Add-on (wt%)	Horizontal damaged length (mm)	Burning time (s)	Afterglow (s)	Residue (wt%)
Uncoated	–	37	24	20	–
5 QL	1.2	37	25	–	22.0
10 QL	3.7	36	19	–	23.5
20 QL	5.4	35	14	–	48.2
PHMGP/APP	1.3	36	20	–	16.2
APP	1.3	37	24	–	8.4
PHMGP/α-ZrP	1.3	37	25	–	10.5

(12 s). Furthermore, no afterglow phenomenon was observed on the coated fabrics, and the entire fabric structure was preserved after burning, while the uncoated fabric left no residue on the sample holder. The decreased burning time and disappearing afterglow for the coated fabric could be attributed to the catalytic charring by the acid sites in the assembly coating and the rapid formation of thermally stable char under the protection of the nanobrick wall coating. As shown in Fig. 6, the 5-QL-coated fabric was completely damaged with 22.0 wt% residue left, while the 10 QLs left some undamaged areas at the sample edge (horizontal length: 1 mm), and its residual char was 23.5 wt%. When the QL number increased to 20, some undamaged areas appeared near the fire source, and the fabric left a longer horizontal undamaged length (35 mm); even the left residue significantly increased to 48.2 wt%. This 20-QL nanobrick wall coating (5.4 wt%) leaves more residues after burning than other intumescent coating systems with similar add-ons (Fang et al. 2015b; Li et al. 2011), indicating that this unique nanobrick wall coating has an excellent flame-retardant effect on cotton fabric. Interestingly, the damaged area in all coated fabrics also maintains the fabric structure, as shown in Fig. 6.

In order to highlight the advantage of this nanobrick wall coating, the flame retardancy of the PHMGP/APP-, PHMGP/α-ZrP- and pure APP-coated fabrics (1.3 wt% add-on) was further investigated and compared with the 5-QL PHMGP/APP/PHMGP/α-ZrP-coated fabric (1.2 wt% add-on). As shown in Fig. 6, the PHMG/APP-coated fabric burned with a bright white fire for 20 s and 16.2 wt% residue with a 1-mm undamaged area left horizontally after the fire had died out. The pure APP-coated fabric also showed a bright white flame that lasted for 24 s. However, it only left 8.4 wt% residue char after burning. For the PHMGP/α-ZrP-coated fabric, the flame presented as fiery red and continued for 25 s, and the remaining residue was 10.5 wt%. As compared to the 5-QL PHMGP/APP/PHMGP/α-ZrP-coated fabric, the PHMGP/APP- and pure APP-coated fabrics presented shorter burning times and similar damaged areas. In spite of this, this 5-QL nanobrick wall-coated fabric left much more residue than the PHMGP/APP-, PHMGP/α-ZrP- and pure APP-coated fabrics.

SEM was further performed to observe the surface morphologies of the cotton fabrics after VFT. Photographs of the post-burn uncoated fabric were omitted because of the complete consumption during the flammability test. For the PHMGP/APP-, PHMGP/α-ZrP- and pure APP-coated fabrics, the residues left after burning still retained the intact wave structure (see Fig. 7). However, at higher magnification, it could be found that cotton fibers shrank to some extent. Moreover, few expanding bubbles appeared on the surface of the cotton fiber residue. For the PHMGP/α-ZrP-coated fabric, a rough and dense thermal barrier with nanosheet-filled formed on the surface of residue char. Despite this, since PHMGP alone has a weak catalytic charring effect on cotton fabric, cotton fibers still withered. In contrast, the post-burn residues for all PHMGP/APP/PHMGP/α-ZrP-coated fabrics kept the original shape of the wave structure, as shown in Fig. 7. For previously reported nanobrick wall systems, although the treated samples partly retained the wave structure, the cotton fibers seriously shrank and curled up after burning. However, for our unique nanobrick wall coating, all coated fabrics kept the original shape of the fiber strands, which could be observed at high magnification. After

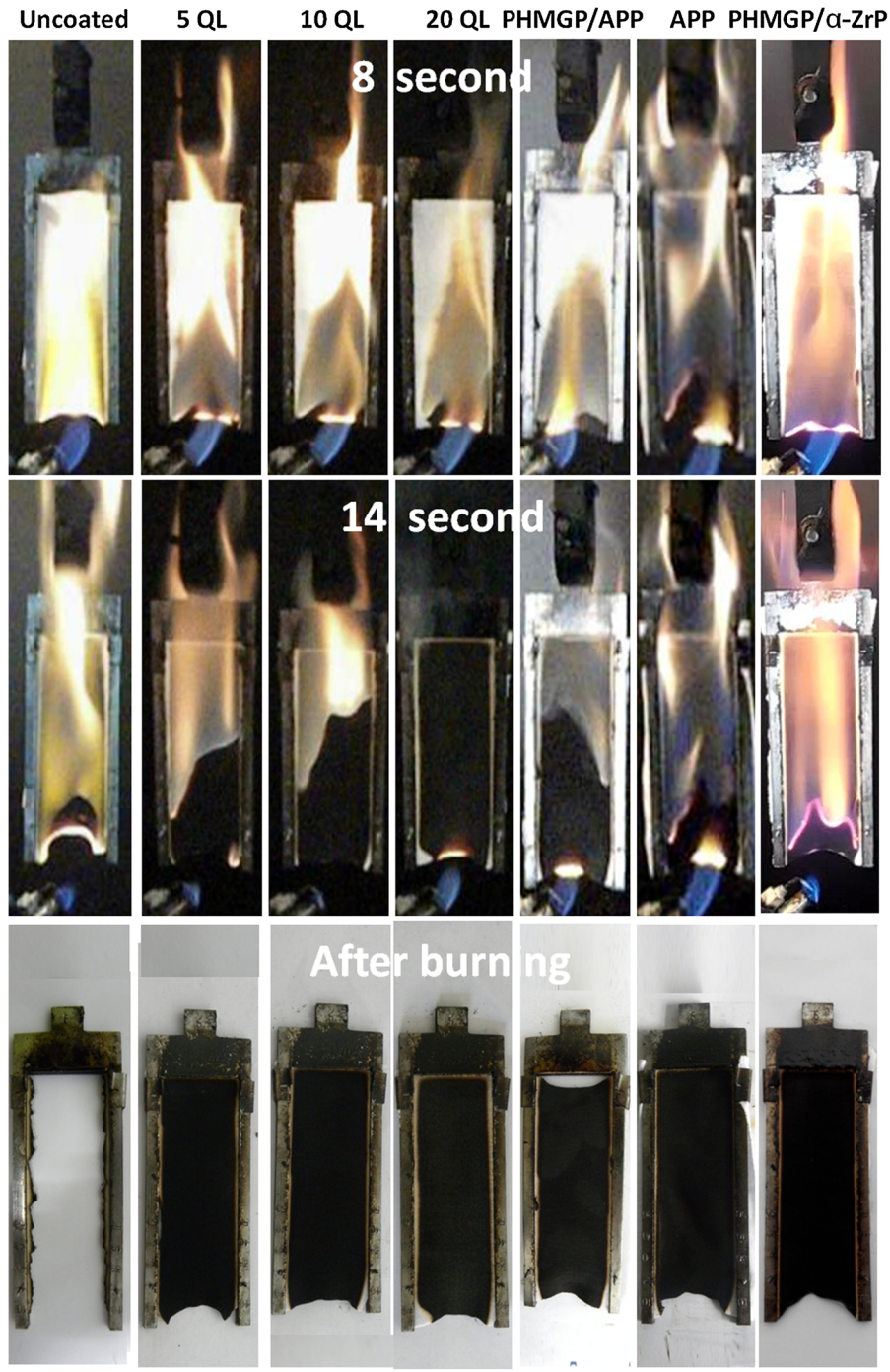

Fig. 6 Images of the uncoated and coated fabrics recorded at 8 and 14 s and after burning

burning, abundant large bubbles were generated at the sticking joints of cotton fibers as the result of an intumescent effect. Flexible polyelectrolytes (PHMGP and APP) tend to gather at the junction, while α-ZrP nanoplatelets with large width migrate into these narrow spaces with difficulty. PHMGP and APP catalyzed the dehydration and carbonization of cellulose by releasing phosphoric acid to form

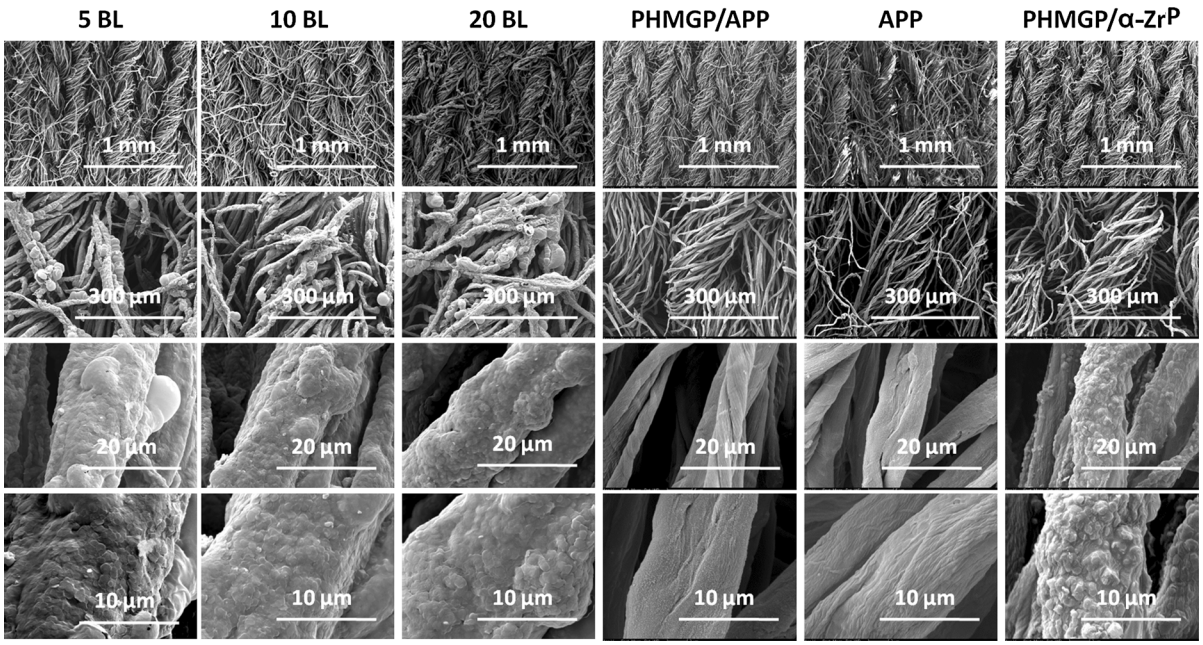

Fig. 7 The SEM images of the uncoated and coated fabrics after VFT

graphitized char (Fang et al. 2015a), which was further swollen by the incombustible volatiles from the intumescent components. However, these bubbles were prone to rupture without the barrier action of α-ZrP nanoplatelets. Additionally, there appeared to be plentiful minute wells without any rupture on the surface of cotton fibers covered by the complete nanobrick wall. When exposed to fire, the polymer mortars transformed into phosphorus-rich thermostable char, which could bond the α-ZrP nanoplatelets, forming a thermostable nanobrick wall structure. Additionally, the Zr^{4+} on the nanoplatelets may unite with the phosphate group from polymer mortars to form zirconium–phosphate bridges that lead to a reinforced nanobrick wall structure (Yang et al. 2008). Therefore, non-flammable gas released from polymer mortars becomes trapped within the interlayers rather than swelling to form larger bubbles observed at the sticking joints of cotton fibers. Significantly, the nanobrick wall as a toughened barrier layer can effectively shield the internal fiber substrate from external heat and oxygen. All these results indicate that this unique nanobrick wall architecture consists of organic intumescent components (PHMGP and APP) and inorganic α-ZrP nanoplatelets, which combine catalytic charring with an inorganic barrier action, can have an enhanced flame-retardant effect on cotton fabric.

FTIR spectroscopy was employed to investigate the chemical composition of the coated fabrics' residue chars left after VFT. As shown in Fig. 8, in the case of the residues from the 5 and 10 QL, no characteristic signals of C–O–C in cellulose are observed in the spectra, but an absorption peak of the C–C chain at

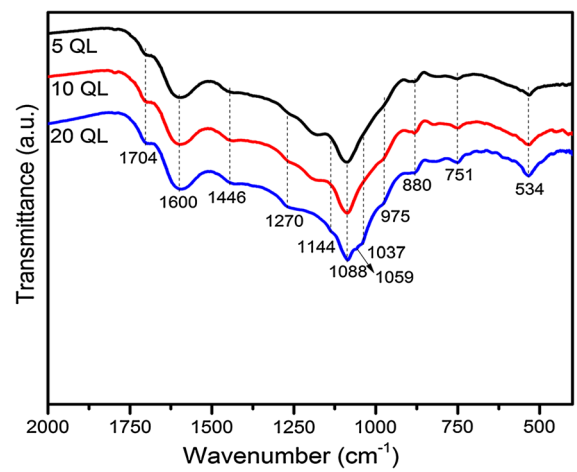

Fig. 8 The FTIR spectra of the post-burn residues of the uncoated and coated fabrics after VFT

1446 cm^{-1} appears. It indicates that the cellulose in cotton fabric is dehydrated by the α-ZrP, and phosphoric acid is released to form carbonaceous char during burning. What is more, these residues also exhibit obvious peaks at 1704 and 1600 cm^{-1}, attributed to the absorption bands of unsaturated C=O and aromatic rings, respectively. The result suggests that cellulose is pyrolyzed and aromatized to form graphitized char, which is thermostable at high temperatures under the barrier effect of the reinforced nanobrick wall structure as "a sealed microreactor." The presence of phosphate can be confirmed by the signals at 1270 and 880 cm^{-1}, ascribed to the absorption of P=O and P–O–P, respectively (Ke et al. 2011). In addition, the characteristic peaks of α-ZrP can also be distinguished at 1088, 751 and 534 cm^{-1}, which are attributed to the P–O–P stretching and deformation modes of PO_4 (Hajipour and Karimi 2014; Tarafdar et al. 2006). Remarkably, besides the above-mentioned signals, the residue from 20 QL also exhibits some weak characteristic signals of C–O–C at 1144, 1059, 1037 and 975 cm^{-1} (Chung et al. 2004), suggesting that cellulose chains cannot be completely dehydrated and aromatized to form graphitized char. As a result, a portion of the cellulose in 20 QL-coated fabric may still be undamaged in a short burning time (14 s) after testing. Therefore, the 20-QL coating as a strong nanobrick wall structure can effectively protect the inside of cotton from fire.

Conclusions

In this study, the PHMGP/APP/PHMGP/α-ZrP QL nanocoating was constructed on cotton fabric to achieve effective flame-retardant treatment via the LBL assembly technique. Characterizations of XRD and ATR-FTIR indicate that the assembly coating grows linearly during the LBL process. The TGA results show that the assembly coating could effectively improve the thermal stability of cotton. In the MCC test, the PHRR and THR values of the coated fabrics are smaller than those of the uncoated ones. In the VFT test, the coated fabric exhibits a decreased buring time, disappearing afterglow phenomenon and remarkably enhanced residue char left with respect to the uncoated one. Furthermore, the PHMGP/APP/PHMGP/α-ZrP-coated fabric has an enhanced flame-retardant property compared to the PHMGP/APP-, PHMGP/α-ZrP- and APP-coated fabrics. SEM photographs indicate that this unique nanobrick wall as a toughened barrier layer could effectively protect the internal fiber substrate during burning. FTIR spectra of the residue char show that cellulose is catalyzed, forming thermostable graphitized char under the barrior effect of the reinforced nanobrick wall structure. This work demonstrates the flame-retardant coating composed of inorganic nanoplatelet and organic intumescent materials, which can provide an effective alternative to the current flame-retardant treatment on cotton fabric.

Acknowledgments The authors are grateful for the financial support from the National Natural Science Foundation of China (No. 51303182).

References

Alongi J, Ciobanu M, Malucelli G (2011a) Novel flame retardant finishing systems for cotton fabrics based on phosphorus-containing compounds and silica derived from sol–gel processes. Carbohydr Polym 85:599–608. doi:10.1016/j.carbpol.2011.03.024

Alongi J, Tata J, Frache A (2011b) Hydrotalcite and nanometric silica as finishing additives to enhance the thermal stability and flame retardancy of cotton. Cellulose 18:179–190. doi:10.1007/s10570-010-9473-z

Alongi J, Brancatelli G, Rosace G (2012a) Thermal properties and combustion behavior of POSS- and bohemite-finished cotton fabrics. J Appl Polym Sci 123:426–436. doi:10.1002/App.34476

Alongi J, Colleoni C, Malucelli G, Rosace G (2012b) Hybrid phosphorus-doped silica architectures derived from a multistep sol–gel process for improving thermal stability and flame retardancy of cotton fabrics. Polym Degrad Stab 97:1334–1344. doi:10.1016/j.polymdegradstab.2012.05.030

Alongi J, Colleoni C, Rosace G, Malucelli G (2014) Sol–gel derived architectures for enhancing cotton flame retardancy: effect of pure and phosphorus-doped silica phases. Polym Degrad Stab 99:92–98. doi:10.1016/j.polymdegradstab.2013.11.020

Apaydin K, Laachachi A, Ball V, Jimenez M, Bourbigot S, Toniazzo V, Ruch D (2014) Intumescent coating of (polyallylamine–polyphosphates) deposited on polyamide fabrics via layer-by-layer technique. Polym Degrad Stab 106:158–164. doi:10.1016/j.polymdegradstab.2014.01.006

Berndt P, Kurihara K, Kunitake T (1992) Adsorption of poly(styrenesulfonate) onto an ammonium monolayer on mica—a surface forces study. Langmuir 8:2486–2490. doi:10.1021/La00046a022

Cain AA, Nolen CR, Li YC, Davis R, Grunlan JC (2013) Phosphorous-filled nanobrick wall multilayer thin film eliminates polyurethane melt dripping and reduces heat

release associated with fire. Polym Degrad Stab 98:2645–2652. doi:10.1016/j.polymdegradstab.2013.09.028
Cain AA, Murray S, Holder KM, Nolen CR, Grunlan JC (2014a) Intumescent nanocoating extinguishes flame on fabric using aqueous polyelectrolyte complex deposited in single step. Macromol Mater Eng 299:1180–1187. doi:10.1002/mame.201400022
Cain AA, Plummer MGB, Murray SE, Bolling L, Regev O, Grunlan JC (2014b) Iron-containing, high aspect ratio clay as nanoarmor that imparts substantial thermal/flame protection to polyurethane with a single electrostatically-deposited bilayer. J Mater Chem A 2:17609–17617. doi:10.1039/c4ta03541k
Carosio F, Alongi J, Malucelli G (2011) Alpha-zirconium phosphate-based nanoarchitectures on polyester fabrics through layer-by-layer assembly. J Mater Chem 21:10370–10376. doi:10.1039/C1jm11287b
Carosio F, Alongi J, Malucelli G (2012) Layer by layer ammonium polyphosphate-based coatings for flame retardancy of polyester–cotton blends. Carbohydr Polym 88:1460–1469. doi:10.1016/j.carbpol.2012.02.049
Carosio F, Di Blasio A, Alongi J, Malucelli G (2013) Green DNA-based flame retardant coatings assembled through layer by layer. Polymer 54:5148–5153. doi:10.1016/j.polymer.2013.07.029
Chen H, Muller MB, Gilmore KJ, Wallace GG, Li D (2008) Mechanically strong, electrically conductive, and biocompatible graphene paper. Adv Mater 20:3557. doi:10.1002/adma.200800757
Chung C, Lee M, Choe E (2004) Characterization of cotton fabric scouring by FT-IR ATR spectroscopy. Carbohydr Polym 58:417–420. doi:10.1016/j.carbpol.2004.08.005
Cobo S, Molnar G, Real JA, Bousseksou A (2006) Multilayer sequential assembly of thin films that display room-temperature spin crossover with hysteresis. Angew Chem Int Ed 45:5786–5789. doi:10.1002/anie.200601885
Dawidczyk TJ, Walton MD, Jang WS, Grunlan JC (2008) Layer-by-layer assembly of UV-resistant poly(3,4-ethylenedioxythiophene) thin films. Langmuir 24:8314–8318. doi:10.1021/La800967x
Decher G, Hong JD (1991) Buildup of ultrathin multilayer films by a self-assembly process. 1. Consecutive adsorption of anionic and cationic bipolar amphiphiles on charged surfaces. Makromol Chem Macromol Symp 46:321–327. doi:10.1002/masy.19910460145
Fang F et al (2015a) Construction of intumescent flame retardant and antimicrobial coating on cotton fabric via layer-by-layer assembly technology. Surf Coat Technol 276:726–734. doi:10.1016/j.surfcoat.2015.05.023
Fang F et al (2015b) Intumescent flame retardant coatings on cotton fabric of chitosan and ammonium polyphosphate via layer-by-layer assembly. Surf Coat Technol 262:9–14. doi:10.1016/j.surfcoat.2014.11.011
Finnemore A, Cunha P, Shean T, Vignolini S, Guldin S, Oyen M, Steiner U (2012) Biomimetic layer-by-layer assembly of artificial nacre. Nat Commun 3:966–971. doi:10.1038/Ncomms1970
Ford ENJ, Mendon SK, Thames SF, Rawlins JW (2010) X-ray diffraction of cotton treated with neutralized vegetable oil-based macromolecular crosslinkers. J Eng Fibers Fabr 5:10–20
Guin T, Cho JH, Xiang FM, Ellison CJ, Grunlan JC (2015) Water-based melanin multilayer thin films with broadband UV absorption. ACS Macro Lett 4:335–338. doi:10.1021/acsmacrolett.5b00080
Hajipour AR, Karimi H (2014) Zirconium phosphate nanoparticles as a remarkable solid acid catalyst for selective solvent-free alkylation of phenol. Chin J Catal 35:1136–1147. doi:10.1016/s1872-2067(14)60060-7
Hongdian L, Wilkie CA (2011) The influence of alpha-zirconium phosphate on fire performance of EVA and PS composites. Polym Adv Technol 22:1123–1130. doi:10.1002/pat.1923
Horrocks AR (2011) Flame retardant challenges for textiles and fibres: new chemistry versus innovatory solutions. Polym Degrad Stab 96:377–392. doi:10.1016/j.polymdegradstab.2010.03.036
Horrocks AR, Nazare S, Masood R, Kandola B, Price D (2011) Surface modification of fabrics for improved flash-fire resistance using atmospheric pressure plasma in the presence of a functionalized clay and polysiloxane. Polym Adv Technol 22:22–29. doi:10.1002/Pat.1707
Huang GB, Liang HD, Wang X, Gao JR (2012a) Poly(acrylic acid)/clay thin films assembled by layer-by-layer deposition for improving the flame retardancy properties of cotton. Ind Eng Chem Res 51:12299–12309. doi:10.1021/ie300820k
Huang GB, Yang JG, Gao JR, Wang X (2012b) Thin films of intumescent flame retardant-polyacrylamide and exfoliated graphene oxide fabricated via layer-by-layer assembly for improving flame retardant properties of cotton fabric. Ind Eng Chem Res 51:12355–12366. doi:10.1021/ie301911t
Kandola BK, Horrocks AR, Horrocks S (2001) Complex char formation in flame-retarded fibre-intumescent combinations. Part V. Exploring different fibre/intumescent combinations. Fire Mater 25:153–160. doi:10.1002/Fam.765a
Ke C, Li J, Fang K, Zhu Q, Zhu J, Yan Q (2011) Enhancement of a hyperbranched charring and foaming agent on flame retardancy of polyamide 6. Polym Adv Technol 22:2237–2243. doi:10.1002/pat.1751
Kim YS, Harris R, Davis R (2012) Innovative approach to rapid growth of highly clay-filled coatings on porous polyurethane foam. ACS Macro Lett 1:820–824. doi:10.1021/mz300102h
Laachachi A, Ball V, Apaydin K, Toniazzo V, Ruch D (2011) Diffusion of polyphosphates into (poly(allylamine)–montmorillonite) multilayer films: flame retardant-intumescent films with improved oxygen barrier. Langmuir 27:13879–13887. doi:10.1021/la203252q
Laufer G, Kirkland C, Morgan AB, Grunlan JC (2012) Intumescent multilayer nanocoating, made with renewable polyelectrolytes, for flame-retardant cotton. Biomacromolecules 13:2843–2848. doi:10.1021/bm300873b
Li YC, Schulz J, Grunlan JC (2009) Polyelectrolyte/nanosilicate thin-film assemblies: influence of pH on growth, mechanical behavior, and flammability. ACS Appl Mater Interfaces 1:2338–2347. doi:10.1021/am900484q
Li YC et al (2010) Flame retardant behavior of polyelectrolyte–clay thin film assemblies on cotton fabric. ACS Nano 4:3325–3337. doi:10.1021/nn100467e
Li Y-C, Mannen S, Morgan AB, Chang S, Yang Y-H, Condon B, Grunlan JC (2011) Intumescent all-polymer multilayer

nanocoating capable of extinguishing flame on fabric. Adv Mater 23:3926. doi:10.1002/adma.201101871

Li YC, Kim YS, Shields J, Davis R (2013) Controlling polyurethane foam flammability and mechanical behaviour by tailoring the composition of clay-based multilayer nanocoatings. J Mater Chem A 1:12987–12997. doi:10.1039/C3ta11936j

Li Y-C, Yang Y-H, Shields JR, Davis RD (2015) Layered double hydroxide-based fire resistant coatings for flexible polyurethane foam. Polymer 56:284–292. doi:10.1016/j.polymer.2014.11.023

Liu YY, Wang XW, Qi KH, Xin JH (2008) Functionalization of cotton with carbon nanotubes. J Mater Chem 18:3454–3460. doi:10.1039/B801849a

Liu A, Walther A, Ikkala O, Belova L, Berglund LA (2011) Clay nanopaper with tough cellulose nanofiber matrix for fire retardancy and gas barrier functions. Biomacromolecules 12:633–641. doi:10.1021/bm101296z

Liu X-Q, Wang D-Y, Wang X-L, Chen L, Wang Y-Z (2013) Synthesis of functionalized alpha-zirconium phosphate modified with intumescent flame retardant and its application in poly(lactic acid). Polym Degrad Stab 98:1731–1737. doi:10.1016/j.polymdegradstab.2013.06.001

Park YT, Ham AY, Grunlan JC (2010) High electrical conductivity and transparency in deoxycholate-stabilized carbon nanotube thin films. J Phys Chem C 114:6325–6333. doi:10.1021/Jp911985g

Reddy PRS, Agathian G, Kumar A (2005) Ionizing radiation graft polymerized and modified flame retardant cotton fabric. Radiat Phys Chem 72:511–516. doi:10.1016/j.radphyschem.2004.03.015

Sehaqui H, Kochumalayil J, Liu A, Zimmermann T, Berglund LA (2013) Multifunctional nanoclay hybrids of high toughness, thermal, and barrier performances. ACS Appl Mater Interfaces 5:7613–7620. doi:10.1021/am401928d

Shuai M, Mejia AF, Chang Y-W, Cheng Z (2013) Hydrothermal synthesis of layered α-zirconium phosphate disks: control of aspect ratio and polydispersity for nano-architecture. CrystEngComm 15:1970. doi:10.1039/c2ce26402a

Stevens B, Dessiatova E, Hagen DA, Todd AD, Bielawski CW, Grunlan JC (2014) Low-temperature thermal reduction of graphene oxide nanobrick walls: unique combination of high gas barrier and low resistivity in fully organic polyelectrolyte multilayer thin films. ACS Appl Mater Interfaces 6:9942–9945. doi:10.1021/Am502889w

Sue HJ, Gam KT, Bestaoui N, Spurr N, Clearfield A (2004) Epoxy nanocomposites based on the synthetic alpha-zirconium phosphate layer structure. Chem Mater 16:242–249. doi:10.1021/Cm030441s

Tang ZY, Kotov NA, Magonov S, Ozturk B (2003) Nanostructured artificial nacre. Nat Mater 2:U413–U418. doi:10.1038/Nmat906

Tarafdar A, Panda AB, Pradhan NC, Pramanik P (2006) Synthesis of spherical mesostructured zirconium phosphate with acidic properties. Microporous Mesoporous Mater 95:360–365. doi:10.1016/j.micromeso.2006.05.008

Tian X et al (2010) Mesoporous zirconium phosphate from yeast biotemplate. J Colloid Interface Sci 343:344–349. doi:10.1016/j.jcis.2009.11.037

Trobajo C, Khainakov SA, Espina A, Garcia JR (2000) On the synthesis of alpha-zirconium phosphate. Chem Mater 12:1787–1790. doi:10.1021/Cm0010093

Ullah S, Ahmad F (2014) Effects of zirconium silicate reinforcement on expandable graphite based intumescent fire retardant coating. Polym Degrad Stab 103:49–62. doi:10.1016/j.polymdegradstab.2014.02.016

Wakelyn PJ, Bertoniere NR, French AD, Thibodeaux DP (2007) Cotton fiber chemistry and technology. Taylor & Francis, London

Walther A, Bjurhager I, Malho JM, Ruokolainen J, Berglund L, Ikkala O (2010) Supramolecular control of stiffness and strength in lightweight high-performance nacre-mimetic paper with fire-shielding properties. Angew Chem 49:6448–6453. doi:10.1002/anie.201001577

Wang JZ, Hu Y, Tang Y, Chen ZY (2003) Preparation of nanocomposite of polyaniline and gamma-zirconium phosphate (gamma-ZrP) by power ultrasonic irradiation. Mater Res Bull 38:1301–1308. doi:10.1016/S0025-5408(03)00147-8

Wang JF, Cheng QF, Tang ZY (2012) Layered nanocomposites inspired by the structure and mechanical properties of nacre. Chem Soc Rev 41:1111–1129. doi:10.1039/C1cs15106a

Weiyi X, Ping Z, Lei S, Xin W, Yuan H (2014) Effects of alpha-zirconium phosphate on thermal degradation and flame retardancy of transparent intumescent fire protective coating. Mater Res Bull 49:1–6. doi:10.1016/j.materresbull.2013.08.033

Wu HX, Liu CH, Chen JG, Yang YJ, Chen Y (2010) Preparation and characterization of chitosan/alpha-zirconium phosphate nanocomposite films. Polym Int 59:923–930. doi:10.1002/Pi.2807

Xu T, Zhang LP, Zhong Y, Mao ZP (2014) Fire retardancy and durability of poly(*N*-benzyloxycarbonyl-3,4-dihydroxyphenylalanine)-montmorillonite composite film coated polyimide fabric. J Appl Polym Sci 131:39608–39615. doi:10.1002/App.39608

Yang D, Hu Y, Song L, Nie S, He S, Cai Y (2008) Catalyzing carbonization function of alpha-ZrP based intumescent fire retardant polypropylene nanocomposites. Polym Degrad Stab 93:2014–2018. doi:10.1016/j.polymdegradstab.2008.02.012

Yang YH, Bolling L, Priolo MA, Grunlan JC (2013) Super gas barrier and selectivity of graphene oxide-polymer multilayer thin films. Adv Mater 25:503–508. doi:10.1002/adma.201202951

Yao HB, Tan ZH, Fang HY, Yu SH (2010) Artificial nacre-like bionanocomposite films from the self-assembly of chitosan-montmorillonite hybrid building blocks. Angew Chem 49:10127–10131. doi:10.1002/anie.201004748

Yuan HX, Xing WY, Zhang P, Song L, Hu Y (2012) Functionalization of cotton with UV-cured flame retardant coatings. Ind Eng Chem Res 51:5394–5401. doi:10.1021/ie202468u

Zhang YM, Jiang JM, Chen YM (1999) Synthesis and antimicrobial activity of polymeric guanidine and biguanidine salts. Polymer 40:6189–6198. doi:10.1016/S0032-3861(98)00828-3

Zhang T, Yan HQ, Wang LL, Fang ZP (2013) Controlled formation of self-extinguishing intumescent coating on ramie

fabric via layer-by-layer assembly. Ind Eng Chem Res 52:6138–6146. doi:10.1021/ie3031554

Zheng Z, Qiang L, Yang T, Wang B, Cui X, Wang H (2014) Preparation of microencapsulated ammonium polyphosphate with carbon source- and blowing agent-containing shell and its flame retardance in polypropylene. J Polym Res. doi:10.1007/s10965-014-0443-2